An Enhanced Region-Based Model for Segmentation Images with Intensity Inhomogeneity

Haiping Yu[1,2(✉)] and Xiaoli Lin[3]

[1] Wuhan College of Foreign Languages and Foreign Affairs, Wuhan, China
seapingyu@163.com
[2] City College of Wuhan University of Science and Technology, Wuhan, China
[3] Wuhan University of Science and Technology, Wuhan, China

Abstract. Segmentation of images with intensity inhomogeneity is always challenging due to low resolution, blurred boundaries and poor illumination. Although existing image segmentation methods were widely used, there exists some shortcomings in segmenting intensity inhomogeneous images, such as not considering the spatial interrelation within the central pixel and its neighborhood. Therefore, this paper proposes an enhanced region-based active contour model for segmenting images with intensity inhomogeneity. In this model, a range-based adaptive bilateral filter is utilized to preserve edge structures and resist the noise of the image. Then an effective energy functional is constructed into the level set framework. With the permission of keeping the original shape of the image, a regularization term is utilized to refrain from the process of re-initialization and speed up the curve evolution. In the end, some experiments on synthetic and real images and contrast with the classic segmentation models are executed. The proposed model is more accuracy than other classic models.

Keywords: Image segmentation · Region-based model · Level set

1 Introduction

Image segmentation plays a vital role in image processing and computer vision such as pattern recognition, image analysis and medical diagnosis. However, due to the complete noise, intensity inhomogeneity and lower gray contrast, these features cause it is extremely challenging in many fields. Particularly, the characteristics of intensity inhomogeneity is a huge problem in the segmentation fields. The idea of image segmentation is to split an image into some sub-regions that do not overlap each other. In particular, for each pixel x in the image domain Ω. We assume that the domain of the image contains N non-overlapping Sub-regions, which means that: $\Omega = \cup \Omega_i (i = 1, 2, 3, \ldots\ldots N)$, $\Omega_i \cap \Omega_j = \Phi$, $\forall i \neq j$. Many of segmentation methods have been proposed, such as fuzzy clustering methods [1–3], deep learning based methods [4–6], and super pixel based methods [7, 8] and active contour methods (ACM) [9–15]. Fuzzy clustering methods work well on noise free images, however, these methods cannot accurately segment images corrupted by severe noise, low contrast and intensity inhomogeneity. Recently, deep learning based methods are currently in a stage of rapid

H. Peng et al. (Eds.): ISICA 2018, CCIS 986, pp. 165–176, 2019.
https://doi.org/10.1007/978-981-13-6473-0_15

development and have been approved in segmentation fields. However, this type of method requires a large number of training sample sets, which is not suitable for a small number of intensity inhomogeneous images, especially medical images. Super pixel segmentation methods generally require preprocessing and are prone to over-segmentation. ACM has been widely used to segmenting images, it is several desirable advantages for segmentation images with intensity inhomogeneity over the above mentioned segmentation methods.

In ACMs, they are divided into two major categories: one is edge-based model and the other is region-based model. Edge-based model uses the gradient of the image to get the segmentation result, which is effective to images with sharp contours. Recent years, region-based ACM and its variant models have been well addressed for image segmentation, which utilizes spatial statistical information to guide the curve evolution. The superiority is that it utilizes the local statistical information and the intensity of image itself in the local region-based models [16]. The Chan-Vese (CV) model, addressed by Chan and Vese in the Ref. [9], is one of the famous region-based model. Later, many region-based segmentation models are addressed to segment intensity inhomogeneous images. In related works, we will introduce some related models.

The rest of this paper is composed as follows: we review three typical region-based methods for image segmentation in Sect. 2. In Sect. 3, we detailed elaborate the proposed model with three subsections. Section 4 analyzes the comparison results with the representative segmentation models on artificial and real images. Finally, in Sect. 5, we end with conclusion and our future work.

2 Related Works

2.1 The CV Model

The CV model, a well-known region-based model, has been proposed by Chan and Vese in 2002. It is on the assumption that there is the same intensity value in two partitions, which refer the target to be segmented and background. Specifically, we use $I(x)$ as the test image and ϕ as its domain, the contour C is the curve, the energy functional is defined as follows:

$$\begin{aligned} E^{CV}(\phi) = \mu \int_{\Omega} \delta(\phi)|\nabla\phi| dxdy + v \int_{\Omega} H(\phi) dxdy \\ + \lambda_1 \int_{in(C)} |I(x,y) - c_1|^2 dxdy + \lambda_2 \int_{out(C)} |I(x,y) - c_2|^2 dxdy \end{aligned} \tag{1}$$

Here, $\mu, \nu, \lambda_1, \lambda_2$ are non-negative constant weight parameters. $I(x, y)$ represents the observed image, $H(\phi)$ is a Heaviside function shown in Eq. (2), and $\delta(\phi)$ (see Eq. (3)) is the derivative of $H(\phi)$. $in(C)$ and $out(C)$ are the region inside and outside of the contour C, respectively.

$$\mathrm{H(x)} = \frac{1}{2}\left[1 + \frac{2}{\pi}\arctan\left(\frac{x}{\varepsilon}\right)\right] \tag{2}$$

$$\delta(\mathrm{x}) = \frac{\partial H(x)}{\partial x} = \frac{\varepsilon}{\pi \cdot (\varepsilon^2 + x^2)} \tag{3}$$

2.2 The Local Image Fitting Model

To accurately segment intensity inhomogeneous images, Zhang et al. constructed a model based on local information, which utilized a truncated Gaussian function as local constraint information. It improved the computational efficiency and reduced the chance of the curve evolution function falling into local optimum. The LIF energy functional is defined as follows:

$$\mathrm{E}^{LIF}(\phi) = \frac{1}{2}\int_{\phi} \left|I(x) - I^{LFI}(x)\right|^2 dx, x \in \Omega \tag{4}$$

Where $I^{LFI}(x)$, named a local fitted image formulation, the mathematical formulation is defined as follows:

$$\mathrm{I}^{LFI} = m_1 H_\varepsilon(\phi) + m_2(1 - H_\varepsilon(\phi)) \tag{5}$$

Here, m_1 and m_2 are respectively the average intensity of inside and outside the region. The definition see the Ref. [17].

2.3 The Local Statistical Active Contour Model (LSACM)

Though the LIF model was more computationally effective in segmenting intensity inhomogeneous images. When the image is disrupted by noise, lower resolution and more overlapping. This model will not perform well. Therefore, Zhang et.al have addressed a new model, named a locally statistical active contour model (LSACM) [18]. In this model, a clever mapping was created, which was mainly used to minimize overlapping. The energy function was defined:

$$E^L_{\theta,B} = \sum\nolimits_{i=1}^{n} \int_{\Omega}\int_{\Omega_i} K_\rho(x,y)\left(\log(\sigma_i) + \frac{(I(y) - B(x)c_i)^2}{2\sigma_i^2}\right)dydx \tag{6}$$

In Eq. (6), $\Omega = \sum_{i=1}^{n} \Omega_i$, with $\Omega_i \cap \Omega_j = \emptyset$, for all $\mathrm{i} \neq \mathrm{j}$, $K_\rho(x,y)$ is the indicator function of local region O_x. ρ controls the size of the local region. $\theta_i = \{c_i, \sigma_i\}, \theta = \{\theta_i, i = 1, \ldots, n\}$.

Compared with CV model and LIF model, this LSACM segment well in intensity inhomogeneous images, especially medical images. However, the model has limitations which is the noise of the image are assumed to be Gaussian distribution. In addition, the model cannot consider the influence of spatial constraint information.

3 The Proposed Model

Base on the above analysis, we address a novel enhanced region-based model, in which edge properties can be well preserved and segmentation results have more accurate. The main idea is to construct a data-driven energy model, which is based on the enhanced range-based bilateral filter. Different from other models, the filter can preserve edge sharpness and reduce noise.

3.1 The Enhanced Region-Based Bilateral Filter

The basic bilateral filter has some merit over other filter technology. It is based on two aspects [19–21]: one is for considering the relationship among the pixels of the image; the other is for considering the image spatial information, which is vital to accurate segmentation.

In our model, we construct an efficient enhanced bilateral filter. For an image $f(x)$, the mathematical expression description is defined as:

$$h(x) = k_r^{-1} \int_{\Omega} f(\xi) c(\xi, x) s(\xi, x, \zeta) d\xi \tag{7}$$

With the normalization

$$k(x) = \int_{\Omega} c(\xi, x) s(\xi, x, \zeta) d\xi \tag{8}$$

And the function of c is used to measure the geometric closeness in the local area; s is used for gauging the spatial information. The definitions are followed as:

$$c(\xi, x) = exp\left(\frac{||\xi - x||^2}{2\sigma_1^2}\right) \tag{9}$$

$$s(\xi, x, \zeta) = exp\left(\frac{||f(\xi) - f(x) - \zeta(x)||^2}{2\sigma_2^2}\right) \tag{10}$$

To boost the robustness of noise, we set a local region as an enhanced filter region. In Eq. (10), the function $\zeta(x)$ controls the scale of the local region. The definition is followed as:

$$\zeta(x) = \begin{cases} \left|f(x) - M\left(\Omega_y\right)\right|, & |x - y| \le \rho \\ = 0, & otherwise \end{cases} \tag{11}$$

Where Ω_y means the neighborhood centered the image of pixel x; $M(\bullet)$ represents the mean intensity value within the neighborhood centered on the pixel x.

3.2 The Energy Model Based on Enhanced Region-Based Bilateral Filter

In this subsection, we propose and analyze the level set energy model in detail. In the proposed model, all notations is followed as:

(1) $I : \Omega \to \mathcal{R}^d$ represents the observed image I, Ω means the domain of the image, d means the dimension of the image;
(2) $\mathcal{C}$ is the closed contour in the domain Ω of I;
(3) $h(x)$ comes from the Eq. (7).
(4) λ_i, (i = 1, 2) are non-negative constants.
(5) f_i, (i = 1, 2) are the average intensity value inside and outside of the closed $\mathcal{C}$, respectively

Therefore, we construct the proposed energy function as follows:

$$\varepsilon = \sum_{i=1}^{2} \lambda_i \int_{\Omega_i} K(x-y)|h(y)I(y) - f_i(x)|^2 dy \tag{12}$$

Where $K(\bullet)$ is an indicator function, the value is 1 in the neighborhood of the pixel, otherwise is zero.

In the domain Ω, we get the energy function:

$$E(\mathcal{C}, f_1, f_2) = \int_{\Omega} \varepsilon(f_1, f_2) + \upsilon|\mathcal{C}| \tag{13}$$

Using the LSF ϕ to replace the contour $\mathcal{C}$, we redefine the equation as:

$$E(\phi, f_1(\mathrm{x}), f_2(\mathrm{x})) = \sum_{i=1}^{2} \lambda_i \int \int K_\rho |h(y)I(y) - f_i|^2 M_i(\phi) dy dx \tag{14}$$

Here, $M_1(\phi) = \mathrm{H}(\phi), M_2(\phi) = 1 - \mathrm{H}(\phi)$. In order to keep the LSF's stability during the curve evolution. In our model, we add a regularization term. Therefore, the final energy function can be rewritten as:

$$\begin{aligned} \mathcal{F}(\phi, f_1, f_2) = \sum_{i=1}^{2} \lambda_i \int \int K_\rho |h(y)I(y) - f_i|^2 M_i(\phi) dy dx \\ + \nu \int \delta|\nabla\phi| dx + \frac{1}{2}\mu \int |\nabla\phi - 1|^2 dx \end{aligned} \tag{15}$$

Here μ and ν are nonnegative constants. Next, we minimize the Eq. (15) by using gradient flow method [22–24] described in Subsect. 3.3.

3.3 Energy Minimization

In Eq. (15), we first fix the implicit function ϕ, and minimize the energy functional about $f_1(x)$ and $f_2(x)$. Therefore, we get the following Euler-lagrange equations:

$$\int K(x-y)M_i(\phi)(h(y)I(y)-f_i(x))^2dy=0, i=1,2 \tag{16}$$

Accordingly, we get the expression about f_i (i = 1, 2):

$$f_i(x)=\frac{K_\rho(x)*[M_i(\phi)h(x)I(x)]}{K_\rho(x)*M_i(\phi)} \tag{17}$$

In fact, the values of $f_i(x)$ (i = 1, 2) are mean value of the intensities within the neighborhood of the pixel x. And the size is related to the parameter $\boldsymbol{\rho}$.

Finally, we get the energy functional about ϕ, by solving the following the equation:

$$\frac{\partial\phi}{\partial t}=-\delta(\phi)(\lambda_1 e_1-\lambda_2 e_2)+\upsilon\delta(\phi)div\left(\frac{\nabla\phi}{|\nabla\phi|}\right)+\mu\left(\nabla^2\phi-div\left(\frac{\nabla\phi}{|\nabla\phi|}\right)\right) \tag{18}$$

And, e_1 and e_2 are followed as:

$$\mathrm{e}_i(x)=\int K_\rho(y-x)|h(x)I(x)-f_i(y)|^2dy, i=1,2 \tag{19}$$

4 Experimental Results

4.1 Experimental on Artificial Images

In the first experiment, we verify the proposed model effectiveness. Figure 1 shows the segmentation results for artificial images and their level set function. The first image has no noise, the latter three images are corrupted by noise. It is obvious that our model can successfully extracts the object boundaries. Their level set functions can keep good stability.

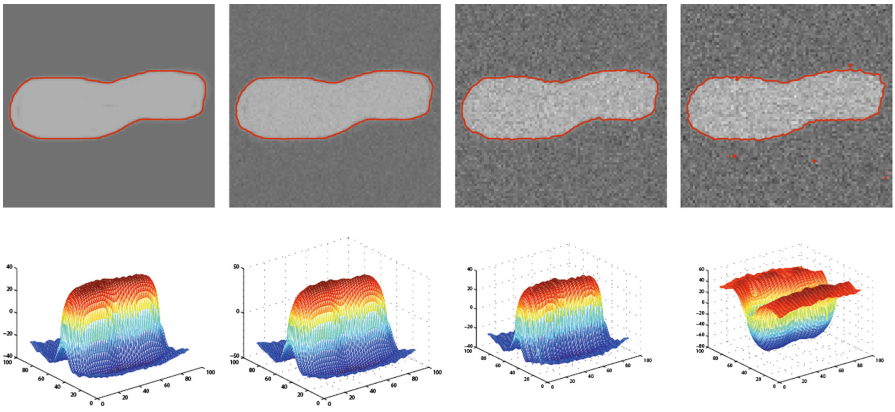

Fig. 1. Segmentation results of our model for artificial image, its noisy image and its level set function.

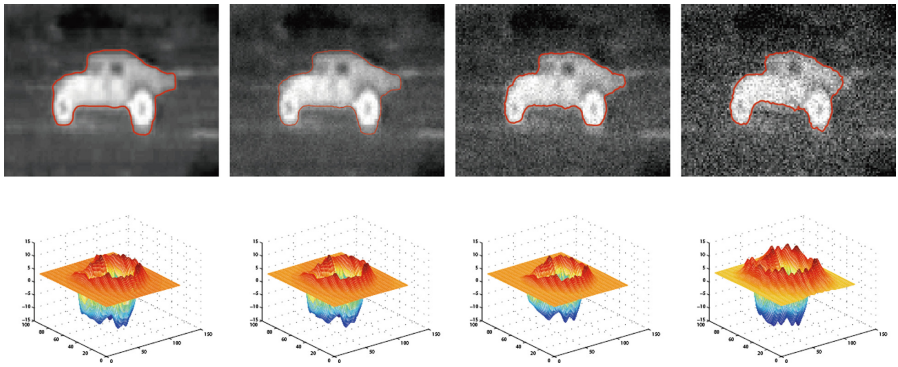

Fig. 2. Segmentation results of our model for synthetic image, its noisy image and its level set function.

In the second experiment, we also evaluated the effectiveness of the proposed model on an edge-blurred image and its noisy image. As shown in Fig. 2, the image boundaries are quite weak. It is clearly shown that our model accurately segments the object shapes.

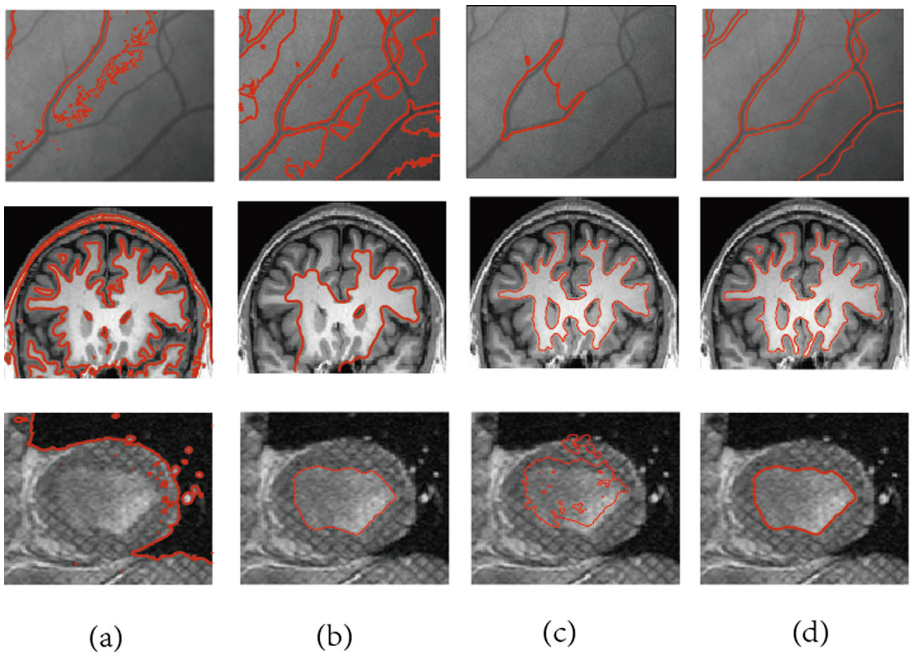

Fig. 3. Comparisons of our model with other classic segmentation models: (a) CV model, (b) LGD model, (c) LSACM, (d) our model.

4.2 Experimental Results

In the third experiment, comparison results in segmenting the real images are executed between the proposed model and other classic models: the CV model [9], the LGD model [25] and the LSACM [18]. As shown in Fig. 3, the CV model has poor performance in segmenting the images. The reason lies in it is based on the global intensity information. In the LGD model, the local image intensities was construct by Gaussian distributions with different means and variances. If we give correct initialization information, then we get more accurate segmentation results as shown in the third image. The LSACM is also suitable for segmenting MRI medical images with intensity inhomogeneity as shown in the second image. By contrast, our model successfully extracts image boundaries for the images as shown in the last column of Fig. 3.

To further verify the performance of the proposed model, in the fourth experiment, we test the proposed model for three images with severe intensity inhomogeneity, the results in Fig. 4 show that the RSF model can accurately segment two images. And our model successfully extracts all the boundaries of the images. For the LVC model [26], it cannot segments the first image, because the image has the feature of poor illumination. The main reason lies that the enhanced range-based bilateral filter can preserve edge sharpness and reduce noise.

We implemented the proposed model in MatlabR2013b. In the proposed model, the main computational time is closely related to the scale of the image. The complexity of the four models' competitive algorithms is $O(N)$, here N represents the number of iteration.

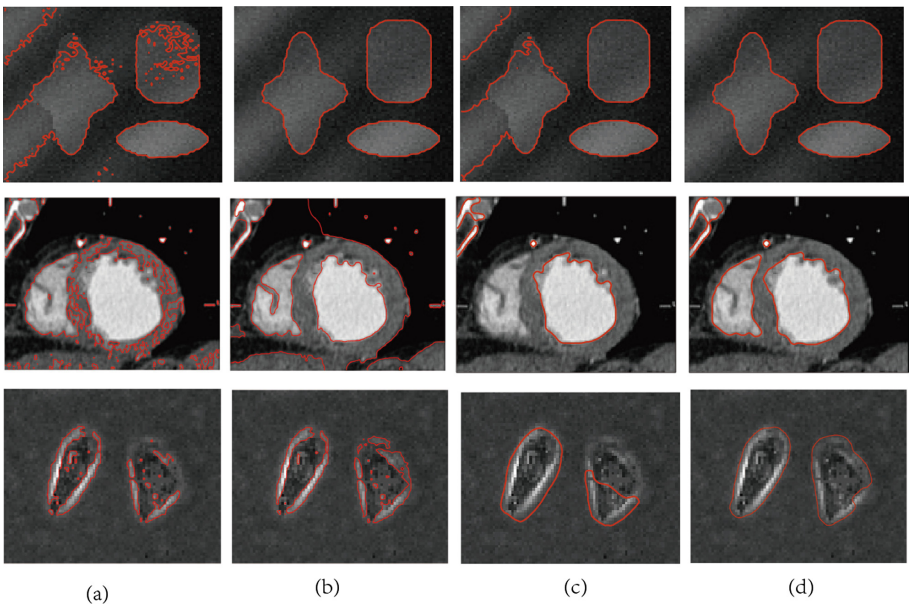

Fig. 4. Comparisons of our model with other classic segmentation models: (a) the CV model, (b) the RSF model, (c) the LVC model, (d) our model.

5 Quantity Analysis

In this section, we evaluate the efficiency of the proposed model using similarity measurement. In segmentation fields, Jaccard similarity (*JI*) coefficient is a well statistic used for measuring similarity between the ground truth and the real segmentation result. The JI can be computed by

$$JI(S_1, S_2) = \frac{|S_1 \cap S_2|}{|S_1 \cup S_2|} \tag{20}$$

In segmentation fields, S_1 and S_2 are the segmented object region and the ground truth, respectively.

Next, we use a synthetic image with different Gaussian noise to evaluate the efficiency of our proposed model as shown in Fig. 5, and the *JI* values are listed in Table 1. When the noise is small, the JI values are relatively similar. As image noise increases, the boundaries of the image become increasingly blurred. The improved bilateral filter can resist the noise and preserve the detail of the image, the CV model cannot resist the noise of the image. For the LCV and the RSF models, when the influence of noise is small, the method can effectively segment the image. However, when the noise is gradually increased, the method cannot resist the influence of noise, and thus cannot be correctly segmented. Obviously, comparison results shows that the proposed model is more efficient than other models shown in Fig. 5.

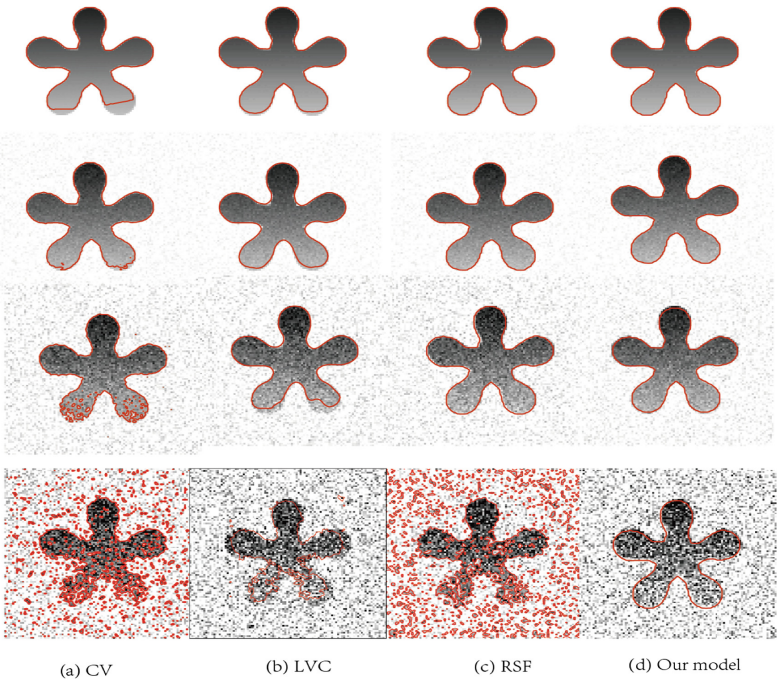

Fig. 5. Comparisons among the CV, the LVC, the RSF model and our model with different noise: (a) the CV model, (b) the LVC model, (c) the RSF model, (d) our model.

Table 1. Comparisons of Jaccard Index with different Gaussian noise.

Line number	CV	LVC	RSF	Our model
Line 1	0.9872	0.9921	0.9799	0.9965
Line 2	0.9821	0.9899	0.9831	0.9913
Line 3	0.8919	0.9822	0.9841	0.9901
Line 4	0.7692	0.7312	0.6954	0.9853

6 Conclusions and Future Works

In this paper, we have proposed an enhanced region-based model for image segmentation. The proposed model efficiently utilizes a range-based adaptive bilateral filter to preserve the sharp edges and reduce the noise of the image. In addition, the model use a regularization term to ensure the regularity of the level set function and to avoid the process of the expensive re-initialization. Comparisons with the well-known models in the literature [9, 10, 18, 25] and [26], the proposed model is more efficient.

In future work, we mainly focus on three directions but not limited: (1) we will utilize intelligent algorithms and hardware resources to enhance the efficiency of the proposed model [27–29]. (2) We will absorb other related fields methods to improve the efficiency of the proposed model, such as image retrieval [30–32] and image super-resolution [33–35].

Acknowledgments. We would like to thank the editors and the reviewers for their pertinent comments. This work was supported in part by the National Natural Science Foundation of China (Grant No. 61502356) and the Hubei Provincial Department of Education Science and Technology Research Project (No. B2016590).

References

1. Chuang, K.S., Tzeng, H.L., Chen, S., et al.: Fuzzy c-means clustering with spatial information for image segmentation. Comput. Med. Imaging Graph. **30**(1), 9–15 (2006)
2. Gong, M., Liang, Y., Shi, J., et al.: Fuzzy c-means clustering with local information and kernel metric for image segmentation. IEEE Trans. Image Process. **22**(2), 573–584 (2013)
3. Han, Y., Shi, P.: An improved ant colony algorithm for fuzzy clustering in image segmentation. Neurocomputing **70**(4–6), 665–671 (2007)
4. Xu, J., Luo, X., Wang, G., et al.: A deep convolutional neural network for segmenting and classifying epithelial and stromal regions in histopathological images. Neurocomputing **191**, 214–223 (2016)
5. Qi, C.R., Su, H., Mo, K., et al.: PointNet: deep learning on point sets for 3D classification and segmentation. Proc. Comput. Vis. Pattern Recognit. (CVPR) **1**(2), 4 (2017)
6. Prasoon, A., Petersen, K., Igel, C., Lauze, F., Dam, E., Nielsen, M.: Deep feature learning for knee cartilage segmentation using a triplanar convolutional neural network. In: Mori, K., Sakuma, I., Sato, Y., Barillot, C., Navab, N. (eds.) MICCAI 2013. LNCS, vol. 8150, pp. 246–253. Springer, Heidelberg (2013). https://doi.org/10.1007/978-3-642-40763-5_31

7. Achanta, R., Shaji, A., Smith, K., Lucchi, A., Fua, P., Süsstrunk, S.: SLIC superpixels compared to state-of-the-art superpixel methods. IEEE Trans. Pattern Anal. Mach. Intell. **34** (11), 2274–2282 (2012)
8. Cheng, J., et al.: Superpixel classification based optic disc and optic cup segmentation for glaucoma screening. IEEE Trans. Med. Imaging **32**(6), 1019–1032 (2013)
9. Chan, T.F., Vese, L.A.: Active contours without edges. IEEE Trans. Image Process. **10**(2), 266–277 (2001)
10. Li, C., Kao, C.Y., Gore, J.C., et al.: Minimization of region-scalable fitting energy for image segmentation. In: IEEE Transactions on Image Processing: A Publication of the IEEE Signal Processing Society, vol. 17, no. 10, p. 1940 (2008)
11. Zhao, Y., Rada, L., Chen, K., et al.: Automated vessel segmentation using infinite perimeter active contour model with hybrid region information with application to retinal images. IEEE Trans. Med. Imaging **34**(9), 1797–1807 (2015)
12. Zhou, S., Wang, J., Zhang, S., Liang, Y., Gong, Y.: Active contour model based on local and global intensity information for medical image segmentation. Neurocomputing **186**, 107–118 (2016)
13. Niu, S., Chen, Q., de Sisternes, L., et al.: Robust noise region-based active contour model via local similarity factor for image segmentation. Pattern Recognit. **61**, 104–119 (2017)
14. Yu, H., He, F., Pan, Y.: A novel region-based active contour model via local patch similarity measure for image segmentation. Multimed. Tools Appl. **77**, 1–23 (2018)
15. Sun, W., Dong, E., Qiao, H.: A fuzzy energy-based active contour model with adaptive contrast constraint for local segmentation. Signal Image Video Process. **12**(1), 91–98 (2018)
16. Haiping, Yu., Huali, Z.: Regularized level set method by incorporating local statistical information and global similarity compatibility for image segmentation. In: Huang, D.-S., Bevilacqua, V., Prashan, P. (eds.) ICIC 2015. LNCS, vol. 9225, pp. 388–399. Springer, Cham (2015). https://doi.org/10.1007/978-3-319-22180-9_38
17. Zhang, K., Song, H., Zhang, L.: Active contours driven by local image fitting energy. Pattern Recognit. **43**(4), 1199–1206 (2010)
18. Zhang, K., Zhang, L., Lam, K.M., et al.: A level set approach to image segmentation with intensity inhomogeneity. IEEE Trans. Cybern. **46**(2), 546–557 (2016)
19. Zhang, B., Allebach, J.P.: Adaptive bilateral filter for sharpness enhancement and noise removal. IEEE Trans. Image Process. **17**(5), 664–678 (2008)
20. Farbman, Z., Fattal, R., Lischinski, D., et al.: Edge-preserving decompositions for multi-scale tone and detail manipulation. ACM Trans. Graph. (TOG) **27**(3), 67 (2008)
21. Kang, X., Li, S., Benediktsson, J.A.: Spectral–spatial hyperspectral image classification with edge-preserving filtering. IEEE Trans. Geosci. Remote Sens. **52**(5), 2666–2677 (2014)
22. Michailovich, O., Rathi, Y., Tannenbaum, A.: Image segmentation using active contours driven by the Bhattacharyya gradient flow. IEEE Trans. Image Process. **16**(11), 2787–2801 (2007)
23. Adams, S., Dirr, N., Peletier, M.A., et al.: From a large-deviations principle to the Wasserstein gradient flow: a new micro-macro passage. Commun. Math. Phys. **307**(3), 791 (2011)
24. Fritzsch, P., Ramos, A.: The gradient flow coupling in the Schrödinger functional. J. High Energy Phys. **2013**(10), 8 (2013)
25. Wang, L., He, L., Mishra, A., et al.: Active contours driven by local Gaussian distribution fitting energy. Signal Process. **89**(12), 2435–2447 (2009)
26. Zhang, K., Zhang, L., Song, H., et al.: Active contours with selective local or global segmentation: a new formulation and level set method. Image Vis. Comput. **28**(4), 668–676 (2010)

27. Zhou, Y., He, F., Qiu, Y.: Dynamic strategy based parallel ant colony optimization on GPUs for TSPs. Sci. China Inf. Sci. **60**(6), 068102 (2017)
28. Zhou, Y., He, F., Qiu, Y.: Optimization of parallel iterated local search algorithms on graphics processing unit. J. Supercomput. **72**(6), 2394–2416 (2016)
29. Alsmirat, M.A., Jararweh, Y., Al-Ayyoub, M., et al.: Accelerating compute intensive medical imaging segmentation algorithms using hybrid CPU-GPU implementations. Multimed. Tools Appl. **76**(3), 3537–3555 (2017)
30. Xia, Z., Wang, X., Zhang, L., et al.: A privacy-preserving and copy-deterrence content-based image retrieval scheme in cloud computing. IEEE Trans. Inf. Forensics Secur. **11**(11), 2594–2608 (2016)
31. Gonde, A.B., Murala, S., Vipparthi, S.K., Maheshwari, R., Balasubramanian, R.: 3D local transform patterns: a new feature descriptor for image retrieval. In: Raman, B., Kumar, S., Roy, P.P., Sen, D. (eds.) Proceedings of International Conference on Computer Vision and Image Processing. AISC, vol. 460, pp. 495–507. Springer, Singapore (2017). https://doi.org/10.1007/978-981-10-2107-7_45
32. Lu, X., Zheng, X., Li, X.: Latent semantic minimal hashing for image retrieval. IEEE Trans. Image Process. **26**(1), 355–368 (2017)
33. Liu, Y., Lu, Y., Yang, X., et al.: Amplified stimulated emission in up conversion nanoparticles for super-resolution nanoscopy. Nature **543**(7644), 229 (2017)
34. Shi, X., Garcia III, G., Van De Weghe, J.C., et al.: Super-resolution microscopy reveals that disruption of ciliary transition-zone architecture causes Joubert syndrome. Nat. Cell Biol. **19**(10), 1178 (2017)
35. Mo, G.C.H., Ross, B., Hertel, F., et al.: Genetically encoded biosensors for visualizing live-cell biochemical activity at super-resolution. Nat. Methods **14**(4), 427 (2017)